Charge transfer in collisions of $B^{2+}(^2S,^2P)$ and $B^{3+}(^1S)$ ions with He atoms below 200 keV

M. Kimura
School of Allied Health Sciences, Yamaguchi University, 755 Ube, Yamaguchi, Japan
and The Institute of Physical and Chemical Research (RIKEN), Wako, Saitama 351-01, Japan

S. Suzuki and N. Shimakura
Department of Chemistry, Niigata University, Niigata, Japan

J. P. Gu, G. Hirsch, and R. J. Buenker
Theoretische Chemie, Bergische Universität-Gesamthochschule Wuppertal, D-42097 Wuppertal, Germany

I. Shimamura
The Institute of Physical and Chemical Research (RIKEN), Wako, Saitama 351-01, Japan
(Received 26 January 1996)

Charge transfer in $B^{2+}(^2S,^2P)$+He and in $B^{3+}(^1S)$+He collisions is studied theoretically by using a semiclassical molecular representation with 8 and 12 molecular channels for B^{2+} and B^{3+} on He systems, respectively, at collision energies between 200 eV and 200 keV for the former and between 600 eV and 50 keV for the latter. The *ab initio* potential curves and nonadiabatic coupling matrix elements are obtained from the multireference single- and double-excitation configuration-interaction (MRD-CI) calculations for the B^{2+}-He system and a pseudopotential-modified configuration-interaction method for the B^{3+}-He system. The present cross sections for charge transfer by the ground state B^{2+} ions are found to have a broad maximum with a magnitude as large as 2×10^{-15} cm^2 at 100 keV and those by an excited $B^{2+}(^2P)$ state are found to be larger by a factor of 6 than those by the ground state in the same energy regime. B^{2+}-excitation cross sections are smaller than those for charge transfer below 1 keV, while they increasingly dominate above this energy. The present total charge-transfer cross section for B^{3+} in collisions with He is similar to that obtained in earlier work by Gargaud *et al.* [J. Phys. B **27**, 3985 (1994)] both in magnitude and energy dependence, but is found to show slightly different $B^{2+}(2s)$ and $B^{2+}(2p)$ production ratio. [S1050-2947(96)00910-9]

PACS number(s): 34.10+x, 34.70.+e, 34.20.−b

I. INTRODUCTION

Charge transfer in collisions of Be^{q+} and B^{q+} ions with H, He, and H_2 targets in a wide range of collision energy is important for applications; in particular, for fusion research, since these ions, which are always present in the Tokamak reactor, are considered to be dominant poison impurities which cause a lowering in temperature as well as fusion yield [1]. Therefore, a knowledge of a complete set of the cross sections for charge transfer by these ions is essential for success in the practical design of a reactor. Unfortunately, however, the cross sections for charge transfer and dynamics are rarely known for these ions, particularly for projectiles in partially stripped ionic states and He and H_2 targets.

Among those studied, the system of [B^{3+}+He] was relatively well studied earlier by several groups in experiment [2–7] and theory [7–13]. Experiments by Zwally and Cable [2] concerned single charge transfer in the energy range from 30 eV/u to 3 keV/u, while Crandall [3] measured charge-transfer cross sections in the energy range between 1.3 and 7.5 keV/u and gave a maximum value of 2×10^{-15} cm^2 for single and of 1.5×10^{-16} cm^2 for double charge transfer. Similar measurements were performed by Gardner *et al.* [4] and Iwai *et al.* [5]. In addition to total-charge-transfer cross sections, Matsumoto *et al.* [6] and Roncin *et al.* [7] studied the energy dependence of the relative population between $B^{2+}(2s)$ (the cross section σ_{2s}) and $B^{2+}(2p)$ (the cross section σ_{2p}) final states. Both studies gave comparable magnitudes, and found that the relative cross sections increased with an increase of the collision energy. But their σ_{2s}/σ_{2p} ratios are larger by 60% than theoretical ratios, as described below. Theoretically, Shipsey, Browne, and Olson [8] carried out calculations based on a four-channel molecular-orbital (MO) expansion method without inclusion of the electron translation factor (ETF) and found an excellent agreement with earlier measurements of Refs. [2] and [3]. Hansen, Dubois, and Nielsen [9] studied charge-transfer processes below 50 keV/u by using a two-center atomic-orbital (AO) expansion method and also including the dynamical electron-correlation effect. Gargaud *et al.* [10] adopted a model potential approach for obtaining molecular states and employed a quantal approach for scattering dynamics by inclusion of four MOs without the ETF. Although their total-charge-transfer cross sections are in good accord with experiments, the σ_{2s}/σ_{2p} ratio is found to be much smaller at all energies studied. Recent studies by Lopez-Castillo and Ornellas [11], Adjouri *et al.* [12], and Gargaud *et al.* [13] all employed the MO representation, and determined charge-transfer cross sections and orientation and alignment parameters below a few keV/u regime. As described, all results for total charge transfer are found to be reasonable in magnitude, but distributions for partial cross sections are not satisfactory in details of the energy dependence and hence, a more careful study is desirable.

For the $[B^{2+}+He]$ system, there is no systematic theoretical nor experimental report except for the recent small-scale calculation by Wang, Toshima, and Lin [14] at energies above 100 keV and one earlier experimental attempt by Gardner *et al.* [4] above 10 keV. In this calculation, Wang, Toshima, and Lin employed a two-center AO expansion method within a one-electron model, and therefore, the result thus obtained should be reasonable at higher energies, but appear to be less accurate as the energy decreases. Hence, the set of cross-section data, particularly for lower energies, is urgently needed [1].

We, therefore, conduct a theoretical study on charge transfer and projectile excitation for these systems in the energy range from 200 eV to 200 keV for the B^{2+}-He and 600 eV to 50 keV for the B^{3+}-He, based on a molecular-state expansion method modified by inclusion of the ETF within a semiclassical framework. We also assess the effect of the excited state on the charge transfer in the $B^{2+}*+He$ system. The processes we deal with are:

(i) ground-state ions,

$$B^{2+}(^2S)+He\rightarrow B^{+}(2^1S,2^1P)+He^{+}(+0.569\ \text{eV}, -9.10\ \text{eV})\ \text{charge transfer}, \tag{1a}$$

$$\rightarrow B^{2+}(^2P)+He,\quad B^{2+}\text{-excitation}, \tag{1b}$$

$$B^{3+}(^1S)+He\rightarrow B^{2+}(^2S,^2P)+He^{+}+>5.55\ \text{eV}\ \text{charge transfer}; \tag{1c}$$

and (ii) excited-state ions,

$$B^{2+}(^2P)+He\rightarrow B^{+}(^3P)+He^{+}+1.94\ \text{eV}\ \text{charge transfer}. \tag{2}$$

The excited $B^{2+}(^2P)$ state, which separates from the ground $B^{2+}(^2S)$ state by 6 eV, possesses a series of sharp avoided crossings with charge-transfer channels, notably at $4.25a_0$ and about $14a_0$, and is expected to display a complex energy dependence in the charge-transfer cross sections, while the ground state has a sharply avoided crossing with a charge-transfer channel near $48a_0$, interchanging their character inside of this region. Hence, it is important to understand the electron-capture mechanisms for both the ground- and excited-state ions, and to determine each cross section accurately. Practically, ion beams produced experimentally by using a particle-impact ionization technique often result in a mixture of unknown fractions of various types of these ionic states when open-shell ions are involved, and thus, a knowledge of each process for collision dynamics would be helpful for accurate experimental analysis [15]. Although we have repeatedly made this remark in the past, some experimental attempts still seem to have a problem in the data analysis due to the mixture of these ground and metastable ions, and hence, this remark still warrants printing.

The present theoretical approach is basically the same as that used in earlier studies (i.e., based on the molecular-state expansion method within a semiclassical formalism for collision energies above 50 eV) [15–17].

TABLE I. Number of reference configurations (N_{ref}) and number of roots (N_{root}) treated in each irreducible representation, with the corresponding numbers of generated (N_{tot}) and selected (N_{sel}) symmetry-adapted functions for a threshold of $1\times10^{-6}\ E_h$ at a bond distance of 2.0 a_0.

States	$N_{\text{ref}}/N_{\text{root}}$	N_{tot}	N_{sel}
$^2A_1$	70/6	259,136	10,190
$^2B_1$	47/4	226,049	8,401
$^4A_1$	57/3	245,897	5,755
$^4B_1$	64/3	249,331	6,033

II. THEORETICAL MODEL

Because some of the details of the present HeB^{2+} molecular-state calculations and dynamical treatment are similar to our earlier work reported elsewhere [15], only a brief summary of the present model relevant to this discussion is provided here.

A. Molecular states and couplings

1. Multireference single- and double-excitation configuration-interaction method for HeB^{2+}

The adiabatic potential curves of HeB^{2+} are obtained by employing the *ab initio* multireference single- and double-excitation configuration interaction (MRD-CI) method [18], with an individual configuration selection for each state under consideration and subsequent energy extrapolation, using the Table CI algorithm [19]. A threshold of $T=1.0\times10^{-6}\ E_h$ (energy in Hartree) is employed, i.e., each configuration generated by single or double excitation from a reference set is checked, whether its energy lowering is equal to or greater than T (then it is included in the first set of configurations) or less than T (then it is discarded, but its lowering contribution is summed up for the extrapolation step). All electrons are considered explicitly. In the present work, the atomic-orbital basis set for the helium atom $(10s5p1d)/[7s4p1d]$ is employed, which is similar to that used by Sunil *et al.* [20] except that the diffuse d function with exponent 0.03 has been deleted. For the boron atom, we used van Duijneveldt's $(13s8p2d)$ basis set [21]. In addition, one s-type and one p-type diffuse function with the exponents of 0.019 and 0.015, respectively, have been added to the above basis set to further improve the quality of the calculated results. Therefore, the final basis set for the boron atom is $(14s9p2d)$ contracted to $[8s5p2d]$. Generally, most of the present asymptotic excitation energies are accurate within a few % compared with experimental values [22]. Further details of our *ab initio* MRD-CI calculations are listed in Tables I and II. The nonadiabatic coupling elements are calculated by using a finite-difference method [23]. This is done using the actually determined wave functions without any extrapolation, but experience shows that this does not lead to any practical problems because the coupling matrix elements depend only very slightly on the size of the wave function [see Fig. 1(a) of Ref. [23]]. Figure 1(a) displays

TABLE II. Leading configurations for each of the eigenfunctions in energetically increasing order at a BHe^{2+} internuclear distance of 2.0 a_0. All B_1 states correspond to Π states, the A_1 states to Σ^+ or Δ.

States	Configurations	States	Configurations
$^2A_1$	$1\sigma^2 2\sigma^2 3\sigma^1$	$^4A_1$	$1\sigma^2 2\sigma^1 3\sigma^1 4\sigma^1$
	$1\sigma^2 2\sigma^2 4\sigma^1$		$1\sigma^2 2\sigma^1 3\sigma^1 5\sigma^1$
	$1\sigma^2 2\sigma^2 5\sigma^1$		$1\sigma^2 2\sigma^1 3\sigma^1 6\sigma^1$
	$1\sigma^2 2\sigma^2 6\sigma^1$		
	$1\sigma^2 2\sigma^2 1\delta^1$		
	$1\sigma^2 2\sigma^1 3\sigma^2$		
$^2B_1$	$1\sigma^2 2\sigma^2 1\pi^1$		
	$1\sigma^2 2\sigma^2 2\pi^1$	$^4B_1$	$1\sigma^2 2\sigma^1 3\sigma^1 1\pi^1$
	$1\sigma^2 2\sigma^2 3\pi^1$		$1\sigma^2 2\sigma^1 4\sigma^1 1\pi^1$
	$1\sigma^2 2\sigma^1 3\sigma^1 1\pi^1$		$1\sigma^2 2\sigma^1 3\sigma^1 2\pi^1$

adiabatic potential curves for the ground and excited initial $[B^{2+}+He]$ states and charge-transfer channels that lie close to the initial channels.

2. Pseudopotential configuration-interaction method for HeB^{3+}

The adiabatic potential energies for HeB^{3+} are obtained by a configuration-interaction method modified by an inclusion of a pseudopotential to describe the atomic $B^{3+}(1s^2)$ core, thus replacing a four-electron system by an explicit two-electron problem. Since the $1s^2$ core has a closed-shell structure and is tight, the pseudopotential technique to describe the core is appropriate and convenient. The pseudopotential used is a Gaussian-type pseudopotential [24], viz.,

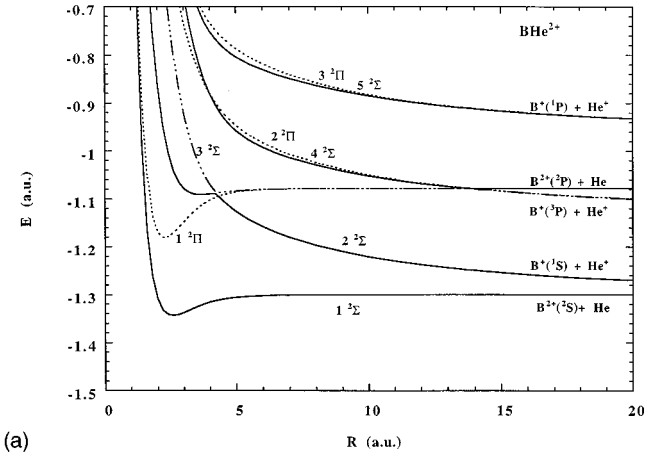

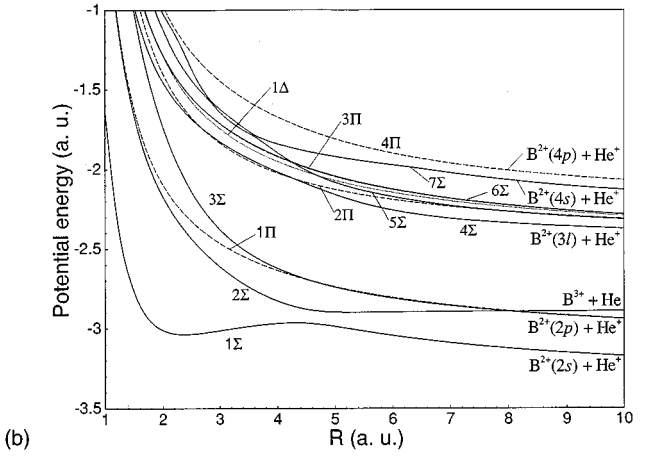

FIG. 1. (a) Adiabatic potentials of the HeB^{2+} system. The energy is given relative to -25.0 a.u.; (b) adiabatic potentials of the HeB^{3+} system. Asymptotic atomic states are indicated in the figure. The energy is given relative to HeB^{5+}.

$$V(R,r)=\sum V_l(R,r)|Y_{lm}\rangle\langle Y_{lm}|, \tag{3}$$

with

$$V_l(R,r)=\sum_l A_l \exp(-\xi_l r^2)-\alpha_d/2(r^2+d^2)^2 - \alpha_q/2(r^2+d^2)^3+2/R, \tag{4}$$

where A_l, ξ_l, α_d, α_q, and d are parameters characterizing the closed shell of an ion (see [24] for details of the definitions). R and r represent the internuclear distance and electronic coordinate, respectively. Slater-type orbitals are employed as basis functions and linear combinations of Slater determinants are used for constructing molecular wave functions. Slater exponents and parameters for the pseudopotential in Eq. (3) are given in Tables III and IV, respectively. Figure 1(b) shows relevant adiabatic potential curves for the $[B^{3+}+He]$. The present asymptotic energies of the adiabatic potentials are better than 0.2% compared with those of ex-

TABLE III. Orbital exponents of the Slater-type-orbital basis functions.

	B^{3+}		He
$2s$	6.909 159	$1s$	4.346
	3.652 416		2.780
	1.853 479		1.450
	0.997 517		
$2p$	2.363 057	$2p$	1.698
	1.438 381		
	1.037 759		
$3s$	1.057 412		
$3p$	1.015		
$3d$	1.001		
$4s$	0.789		
$4p$	0.758		

TABLE IV. Pseudopotential parameters for B^{3+} ion core (in a.u.).

A_0	24.426 318
A_1	−1.523 8484
A_2	−0.769 7479
ξ_0	4.528 4976
ξ_1	4.969 0687
ξ_2	5.0
α_d	0.326
α_q	0.0194
d	3.0

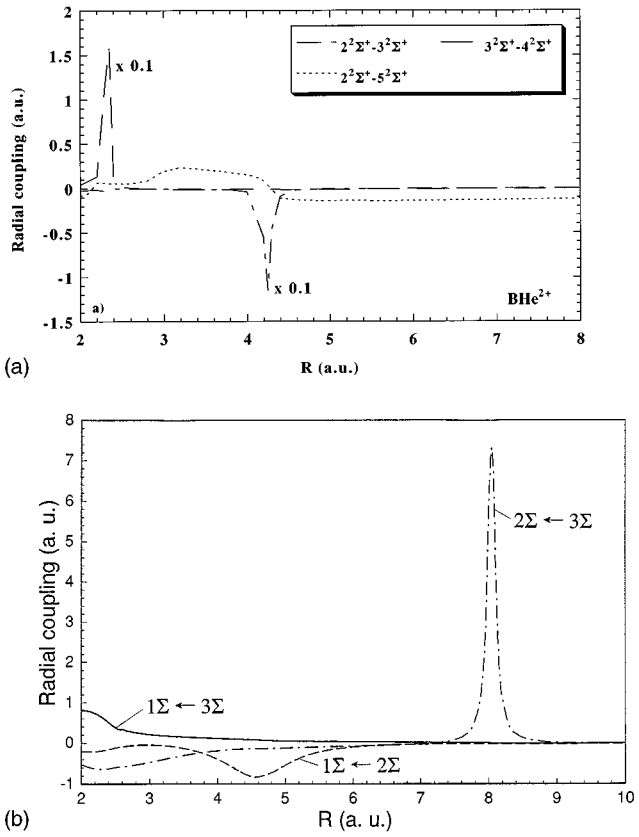

FIG. 2. (a) Nonadiabatic coupling matrix elements for the HeB^{2+} system. The ETF correction up to the first order is included. (b) Nonadiabatic coupling matrix elements for the HeB^{3+} system. The ETF correction up to the first order is also included.

periment [22]. The nonadiabatic coupling matrix elements are evaluated numerically by using the wave functions obtained above.

3. Coupling matrix elements

Representative results for nonadiabatic coupling matrix elements, with inclusion of the first-order ETF correction, for B^{2+}-He and B^{3+}-He are illustrated in Figs. 2(a) and 2(b), respectively. For the B^{2+}-He, as discussed, at $R=48a_0$ and $14a_0$ where the $1^2\Sigma$ and $2^2\Sigma$, and $3^2\Sigma$ and $4^2\Sigma$ possess sharply avoided crossings and they interchange their electronic character (diabatically making $1^2\Sigma$ and $3^2\Sigma$ states the configurations of the $[B^{2+}+He]$ channels within $R=14a_0$), strong radial couplings are seen to peak sharply. The $2^2\Sigma$ and $3^2\Sigma$ potential curves possess a sharply avoided crossing at $R=4.25a_0$, at which point the radial coupling between these states has a sharp peak. This strong coupling, which has a maximum value of about 11.5 a.u., is numerically found to be a dominant mechanism of charge transfer from the excited $B^{2+}(^2P)+He$ channel at the lower energies, i.e., below 500 eV. A remark should be in order that the coupling between $2^2\Sigma$ and $5^2\Sigma$ has a broad peak at $R>4.5a_0$ where no other coupling has a similar size in the same R region. This rather strong coupling at large R is due to the mixing of the states with the same configuration, and is found to make a significant contribution to the $B^+(^1P)$ formation discussed below. It may be also worth a note that second- and higher-order ETF corrections contribute only to reducing a coupling size further down by a few % in this energy region considered, and hence, the present first-order approximation for the ETF treatment is regarded as reasonable.

For the B^{3+}-He, the radial coupling matrix element between the $2^1\Sigma$ and $3^1\Sigma$ states that connects the initial channel and the charge-transfer channel to $B^{2+}(2p)$ possesses a sharp peak around $R=8a_0$ due to the corresponding sharply avoided crossing at this distance. This coupling plays a dominant role for charge transfer to the $B^{2+}(2p)$ state at low energies, but as the energy increases, this coupling is expected to become more diabatic in nature and inefficient. For high energies, the weak coupling between $1^1\Sigma$ and $2^1\Sigma$ at $R=4.3a_0$ becomes increasingly important for the further flux transfer from the initial state to the $2s$ state, causing the $2s$ contribution to be solely dominant. These features of adiabatic potentials and corresponding nonadiabatic couplings are typical for collisions involving highly charged ions, but details are very sensitive to the individual system and different from system to system.

B. Collision dynamics

Semiclassical approach

A semiclassical molecular-state expansion method with a straight-line trajectory was employed to study the collision dynamics for the present cases [17]. Transitions are driven by the nonadiabatic couplings. The total scattering wave function was expanded in terms of products of a molecular electronic state and atomic-type electron translation factors (ETFs). Substituting the total wave function into the time-dependent Schrödinger equation and retaining the ETF correction up to the first order in relative velocity yield a set of first-order coupled differential equations. By solving the coupled equations numerically, we obtain the scattering amplitudes for transitions: the square of an amplitude gives the transition probability, and integration of the probability times the impact parameter over the impact parameter gives the cross section. The molecular states included in the dynamical calculations are the two sets of states as shown in Figs. 1: (1) B^{2+}-He, (i) the ground-state initial channel $[B^{2+}(^2S)+He]:^2\Sigma$, (ii) charge-transfer channels $[B^+(^1S)+He^+]:^2\Sigma$, $[B^+(^3P)+He^+]:^2\Sigma,^2\Pi$, $[B^+(^1P)+He^+]:^2\Sigma,^2\Pi$, and (iii) excitation channels $[B^{2+}(^2P)+He]:^2\Sigma,^2\Pi$, and (2) B^{3+}-He, (i) the initial channel $[B^{3+}(^1S)+He]:^1\Sigma$, (ii) charge-transfer channels $[B^{2+}(2s)+He^+(1s)]:^1\Sigma$, $[B^{2+}(2p)+He^+(1s)]:^1\Sigma,^1\Pi$ and $[B^{2+}(3s,\ 3p,\ 3d$ and $4s)+He^+]:^1\Sigma,^1\Pi,^1\Delta$. In addition, we included $[B^{2+}(4p)+He^+]:^1\Pi$ state to ensure the convergence of the cross section.

III. RESULTS

A. B^{2+} collisions with He

1. Charge transfer by the ground-state B^{2+} ions

The calculated cross sections for charge transfer from the ground state are illustrated in Fig. 3 along with the cross sections for the B^{2+}-excitation process. Both charge-transfer

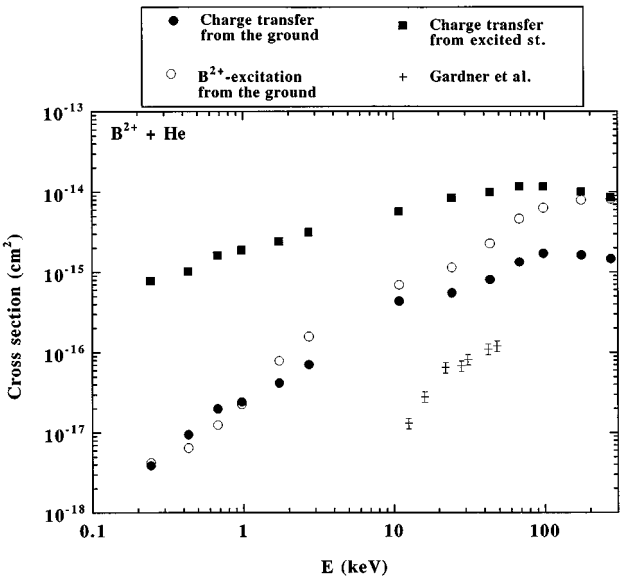

FIG. 3. Charge transfer and excitation cross sections for the B^{2+}-He system. Present work: charge transfer: ■, $B^{2+}(^2P)$; ●, $B^{2+}(^2S)$. B^{2+}-excitation: ○, $B^{2+}(^2S)$. Experiment: +, Gardner *et al.* [4].

and projectile-excitation cross sections by the ground-state ion are found to be large with a magnitude of nearly 2×10^{-15} and 8×10^{-15} cm^2, respectively, at 200 keV, but decrease rather sharply with the decrease of the collision energy, reaching about 10^{-17} cm^2 at 0.4 keV. B^{2+}-excitation cross sections are slightly larger than those for charge transfer above 1 keV. However, their energy dependences and phases in oscillations as functions of energy due to the multichannel interference are very similar because of the strong coupling between the $2\,^2\Sigma$ and $3\,^2\Sigma$ states at $4.25a_0$ which mix the flux well in the outgoing part of the collision. The dominant channels for charge transfer are found to be $B^+(^3P,^1P)$ formations above 10 keV, while the $B^+(^1S)$ formation dominates below 10 keV. In fact, at the lowest energy studied at 0.24 keV, the contribution from the $B^+(^3P,^1P)$ formations constitute slightly over 30%.

The only experimental data for the system by Gardner *et al.* [4] are for the higher-energy side above 10 keV. The measurements are found to be systematically smaller than the present results in magnitude while their energy dependence appears to be similar to the present result above 20 keV. A similar lower trend in magnitude in their measured cross section is seen below for the B^{3+}-He system, and we will make some discussions on this point in the next section. The theoretical result by Wang, Toshima, and Lin [14] covers higher-energy regimes above 100 keV, and at their lowest collision energy where the present study overlaps, the result of Wang, Toshima, and Lin is found to be smaller by a factor of two. Although a reason for this discrepancy is not clear, the one-electron model Wang, Toshima, and Lin adopted may not be appropriate in this intermediate-energy region.

2. Charge transfer by the excited state B^{2+} ions

The charge-transfer cross section from the excited-state ion, included in Fig. 3, is also found to be large and shows weaker energy dependence in the entire region of energy

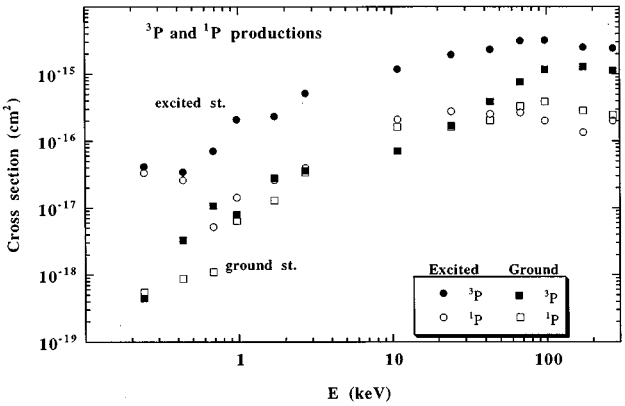

FIG. 4. ^3P and ^1P productions for the B^{2+}-He collisions.

studied than for the ground-state ions. Its value at 1 keV is approximately 2×10^{-15} cm^2. The B^{2+} deexcitation cross section is nearly identical to that of B^{2+} excitation from the ground state above 10 keV as it should be, but as the collision energy decreases and, hence, the magnitude of the cross section decreases below 10^{-17} cm^2, B^{2+} deexcitation and excitation cross sections are found to be somewhat different in the calculation within 30%. This discrepancy at lower energies could happen because the magnitude of the cross section is small and, hence, it is sensitive to every detail of the calculation procedure adopted. The strong coupling between $4\,^2\Sigma$:$[B^+(^3P)+He^+]$ and the initial excited channel influences the story of the behavior of the charge-transfer cross section. As the energy decreases, the coupling between $1\,^2\Sigma$ and $2\,^2\Sigma$ becomes less effective, causing a rather drastic decrease in the B^{2+}-deexcitation and excitation cross sections.

The dominant channel for charge transfer is the $B^+(^1S)$ formation at nearly all energies studied, but the contribution from the $B^+(^3P,^1P)$ formations becomes comparable as collision energy increases. In addition, an oscillatory pattern seen in Fig. 3 has no apparent relation to the two states, implying only weak interference between them. Since a number of channels included in the calculations for the ground and excited states was somewhat different as indicated above, a rigorous comparison between the two may not be significant.

3. Selective ^3P and ^1P formation

Figure 4 illustrates triplet $B^+(^3P)$ and singlet $B^+(^1P)$ state formation from the ground $B^{2+}(^2S)$ and excited $B^{2+}(^2P)$ states. The cross sections for ^3P and ^1P formation from the initial ground state are somewhat similar below 20 keV. The energy gaps between the ground and the B^+ (^3P), and the ground and the $B^+(^1P)$ are different, and this similar magnitude of the cross sections is rather unexpected. However, as we discussed above, the coupling between $2\,^2\Sigma$ and $5\,^2\Sigma$ possesses a broad peak at large $R>4.5a_0$ and this coupling, which is the sole peak among all couplings in this R region, is responsible for making a large contribution to the large $B^+(^1P)$ population. The cross section for ^3P formation, however, begins to increase above 20 keV and eventually becomes dominant by as large as a factor of 5 above 100 keV. For the initial excited state, ^3P formation predominates over singlet formation at nearly all energies. The difference in-

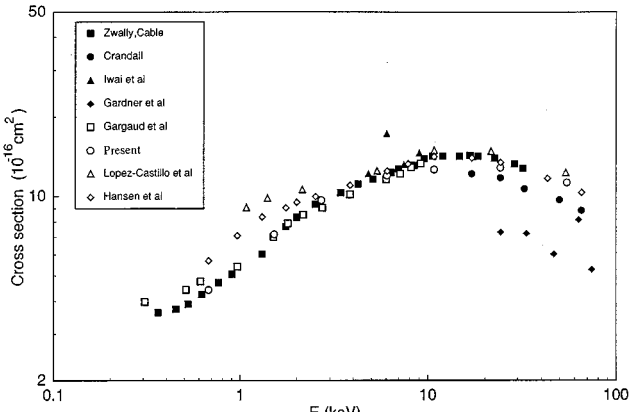

FIG. 5. Charge-transfer cross sections for the B^{3+}-He collisions. Theory: Present work, ○; Gargaud *et al.* [10], □; Lopez-Castillo and Ornellas [11], △; Hanssen, Dubois, and Nielsen [9]; ◇. Experiment: Zwally and Cable [2], ■, Crandall [3], ●; Gardner *et al.* [4], ◆; Iwai *et al.* [5], ▲.

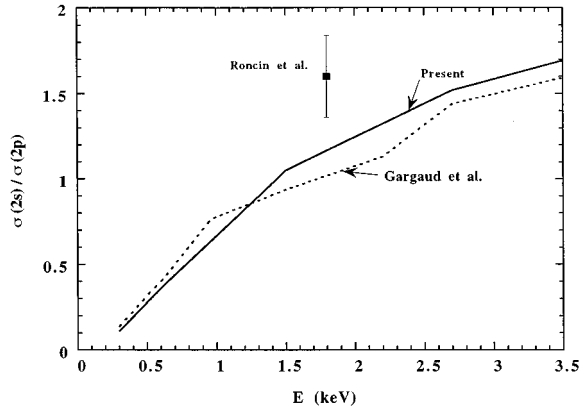

FIG. 6. The ratio of the $2s$ and $2p$ productions in the B^{3+}-He collisions. Theory: Present work; —; Gargaud *et al.* [10]; ---. Experiment: Roncin *et al.* [7], ■.

creases to more than an order of magnitude above 100 keV, while it becomes smaller somewhat below 1 keV. This feature below 1 keV is due to the diabaticity at the crossing between the $[B^{2+}(^2P)+He]$ and $[B^{+}(^3P)+He^{+}]$ states at about $14a_0$, which results in more effective $B^{+}(^1P)$ formation. This knowledge of the ^3P- and ^1P-state formation ratio is important for the selective production of specific ionic states in applied fields such as plasma chemistry. In these ^3P and ^1P formation processes, the Π contributions for both manifolds are nearly the same as or slightly larger than those of Σ states particularly at lower energies, suggesting the importance of rotational couplings.

Lastly, for the initial excited state, contributions to the total-charge-transfer cross section from the initial Σ and Π states are in fact very close to each other in magnitude, because of a strong mixing of the flux between the two degenerate initial channels through strong rotational coupling. Hence, a simple averaging by using results from only one of these initial channels is expected to give a reasonable value of the charge-transfer cross section.

B. B^{3+} collisions with He

1. Total charge transfer

The present charge-transfer cross section is displayed in Fig. 5 along with other theoretical and measured data [2–5,9–11]. The present results are the sum of $2s$ and $2p$ formations. Agreement of the results with earlier data is generally satisfactory. Our results are in excellent agreement with those of Zwally and Cable [2]. However, our results are in poor agreement with those by Gardner *et al.* [4], who show considerably smaller values ($<50\%$) at energies higher than 20 keV. As noted in the preceding section, the experimental data by Gardner *et al.* are smaller for both projectiles reported, and it appears that they might have an experimental problem systematically. Note that one of the experimental data by Iwai *et al.* [5] is far off from the rest of the experimental and theoretical results. Above 20 keV, Crandall [3] carried out the measurement, but his results are smaller by 15–20% although the energy dependence is in good accord. The results calculated by Lopez-Castillas and Ornellas[11] are much larger by more than 30% and show different energy dependence at intermediate to low energies. The result by Hansen, Dubois, and Nielsen [9] appears to agree reasonably well with the measurements and our theory, but the degree of agreement becomes less satisfactory as the energy decreases, with a maximum deviation of 30% from the rest. The agreement between our results and those of Gargaud *et al.* [10] is satisfactory, in particular, at intermediate energies. However, at lower energies our results are in increasingly better accord with the measurement than those of Gargaud *et al.*, which give larger values by as much as 20% from other experimental data.

2. 2s and 2p productions

Figure 6 displays the ratio of $2s/2p$ production along with the theoretical result of Gargaud *et al.* [16] and experimental data [7]. Present magnitude and energy dependences of $2s$ and $2p$ cross sections are found to be simlar to those presented by Gargaud *et al.*, and hence, we do not show them here. Above 1 keV, charge transfer to the $B^{2+}(2s)$ state becomes increasingly dominant, but below this energy, charge transfer to the $B^{2+}(2p)$ state is the main contribution. As discussed above, in the region where $2p$ and $2s$ cross sections are comparable in size, the $2p$ and $2s$ channels interfere with each other and cause out-of-phase oscillatory structures in each cross section. This feature is due to the nature of the radial couplings among the initial and $2s$ and $2p$ channels. Similar values of the $2s$ and $2p$ formations were obtained by Gargaud *et al.* [10,13]. Π contributions through rotational couplings are found to dominate the $B^{2+}(2p)$ formation, by a factor of two or larger, at all energies studied here. A similar finding was noted in Ref. [13].

Although most of the general features in the present cross section agree well with those by Gargaud *et al.*, $2s$ and $2p$ distributions and hence, the ratio σ_{2s}/σ_{2p}, are found to be slightly different. We observed somewhat stronger oscillatory structures in the individual $2s$ and $2p$ cross sections and slightly weaker $2s$ distribution below 1.5 keV, leading to slightly larger ratio although this may not be significant. The experimental ratio obtained by Roncin *et al.* [7] has a larger

value and can be interpreted as a result of the limited angular acceptance angle adopted by the experiment. This point was also noted in Ref. [13]. The present study, based on a larger basis set up to $B^{2+}(n=4)$ manifold, found that the contributions of the $B^{2+}(n=3)$ manifolds to charge transfer are less than 10% even at the highest energy studied and that to $B^{2+}(n=4)$ is even smaller. Hence, the present calculation is considered to be converged within the basis size used.

IV. CONCLUSION

We have studied electron capture in collisions of $B^{2+}(^2S,^2P)$ and $B^{3+}(^1S)$ with He below 200 keV. For the B^{2+}-He system, charge transfer from the ground-state ion is a strong function of energy and rapidly increases from 3×10^{-18} cm^2 at 0.2 keV to 2×10^{-15} cm^2 at 200 keV. We also found that, although the magnitude of the cross section for electron capture by the excited $B^{2+}(2p)$ ions is comparable to that for the ground-state ion at 100 keV, it decreases more slowly as the energy is lowered and becomes nearly constant with a value of 10^{-15} cm^2 below 10 keV. Our results for B^{3+}-He are in good accord with the experimental result and with that by Gargaud *et al.* [10,13]. Charge transfer to the $B^{2+}(2s)$ state becomes dominant above 10 keV, while below this energy, charge transfer to $B^{2+}(2p)$ state contributes significantly. A slight deviation of the present result and that of Gargaud *et al.*, from the experimental data by Roncin *et al.* for the $2s$ and $2p$ ratio was found.

ACKNOWLEDGMENTS

This work was supported in part by RIKEN, Japan (M.K.); a Grant-in-Aid for Science Research in the Priority Area ''Atomic Physics of Multicharged Ions'' (Area No. 239/0523804) from the Ministry of Education, Science and Culture of Japan (N.S.); and Deutsche Forschungsgemeinschaft in the form of a Forschergruppe and Grant No. Bu 450/7-1 (J.P.G., G.H., and R.J.B.). The financial support of the Fonds der Chemischen Industrie is also hereby gratefully acknowledged.

[1] R. Janev, M. F. A. Harrison, and H. W. Drawin, Nucl. Fusion. **29**, 109 (1989).
[2] H. J. Zwally and P. G. Cable, Phys. Rev. A **4**, 2301 (1971).
[3] D. H. Crandall, Phys. Rev. A **16**, 958 (1977).
[4] L. D. Gardner, J. E. Bayfield, P. M. Koch, I. A. Sellin, D. J. Pegg, R. S. Peterson, M. L. Mallory, and D. H. Crandall, Phys. Rev. A **20**, 766 (1979).
[5] T. Iwai, Y. Kaneko, M. Kimura, N. Kobayashi, S. Ohtani, K. Okuno, S. Takagi, H. Tawara, and S. Tsurubuchi, Phys. Rev. A **26**, 105 (1982).
[6] A. Matsumoto, T. Iwai, Y. Kaneko, M. Kimura, N. Kobayashi, S. Ohtani, K. Okuno, S. Takagi, H. Tawara, and S. Tsurubuchi, J. Phys. Soc. Jpn. **52**, 3291 (1983).
[7] P. Roncin, C. Adjouri, M. N. Gaboriaud, L. Guillemot, M. Barat, and N. Andersen, Phys. Rev. Lett. **65**, 3261 (1990).
[8] E. J. Shipsey, J. C. Browne, and R. E. Olson, Phys. Rev. A **15**, 2166 (1977).
[9] J. P. Hansen, A. Dubois, and S. E. Nielsen, Phys. Rev. A **45**, 184 (1992).
[10] M. Gargaud, F. Faija, M. C. Bacchus-Montabonel, and R. McCarroll, J. Phys. B **27**, 3985 (1994).
[11] A. Lopez-Castillo and F. R. Ornellas, Phys. Rev. A **51**, 381 (1995).
[12] C. Adjouri, P. Roncin, M. N. Gaboriand, M. Barat, and N. Andersen, J. Phys. B **27**, 3093 (1994).
[13] M. Gargaud, M. C. Bacchus-Montabonel, R. McCarroll, and T. Grozdanov, J. Phys. B **27**, 4675 (1994).
[14] Y. D. Wang, N. Toshima, and C. D. Lin, Phys. Scr. (to be published).
[15] M. Kimura, J. P. Gu, Y. Li, G. Hirsch, and R. J. Buenker, Phys. Rev. A **49**, 3131 (1995).
[16] N. Shimakura and M. Kimura, Phys. Rev. A **44**, 1659 (1991).
[17] M. Kimura and N. F. Lane, Adv. At. Mol. Opt. Phys. **26**, 76 (1989).
[18] R. J. Buenker and S. D. Peyerimhoff, Theo. Chim. Acta **35**, 33 (1974); *ibid*. **39**, 217 (1975).
[19] R. J. Buenker and R. A. Phillips, J. Mol. Struc. Theochem. **123**, 291 (1985).
[20] K. K. Sunil, J. Lin, H. Siddiqui, P. E. Siska, K. D. Jordan, and R. Shepard, J. Chem. Phys. **78**, 6190 (1983).
[21] F. B. Van Duijneveldt, IBM Research Report No. RJ945, 1971 (unpublished).
[22] C. E. Moore, *Atomic Energy Levels*, Natl. Bur. Stand. (U.S.) NBS Circ. No. 467 (U.S. GPO, Washington, DC, 1949) Vol. 1.
[23] G. Hirsch, P. J. Bruna, R. J. Buenker, and S. D. Peyerimhoff, Chem. Phys. **45**, 335 (1980).
[24] M. Kimura, R. E. Olson, and J. Pascale, Phys. Rev. A **26**, 3113 (1982).